Displays 81 (2024) 102617

Contents lists available at ScienceDirect

Displays

journal homepage: www.elsevier.com/locate/displa

Accommodation-capable holographic waveguide head-up display with extended field of view☆

Woonchan Moon [a], Hosung Jeon [a], Sehwan Na [b], Hwi Kim [b], Joonku Hahn [a,*]

[a] School of Electronic and Electrical Engineering, Kyungpook National University, 80 Daehakro, Buk gu, 41566 Daegu, South Korea
[b] Department of Electronics and Information Engineering, College of Science and Technology, Korea University, Sejong Campus, Sejongro 2511, 30019 Sejong, South Korea

A B S T R A C T

Augmented reality (AR) displays are enhancing user experiences by offering immersive three- dimensional (3D) content, with head-up display (HUD) being a prime application for driving safety. To enable AR-HUDs to provide sufficient information to driver, it is essential to ensure a wide field of view (FOV). Traditional methods like the magnifier principle have limitations stemming from optical aberrations and bulky form factor. Recently, optical waveguide has been used as pupil expander, which has attracted increasing attention as an optical element for compact form factor and exit-pupil expansion. However, waveguide display as exit-pupil expander only offer 2D images with infinite depth, causing mismatch issue between virtual content and real scenes. In this paper, we propose a lensless holographic waveguide display consisting of a laser light source, a spatial light modulator (SLM), a waveguide to generate accommodation-capable images, effectively extending FOV. The key distinction of this research lies in the optical design of the waveguide, which defines multiple shifted copies of the modulated wavefield as replicated virtual SLMs. A formalized algorithm is devised based on a bold assumption that numerous virtual SLMs replicated by a waveguide are considered as a single ultra-high resolution SLM. The effectiveness of the algorithm has been demonstrated through extensive validation through numerical observation simulations and optical experiments. Notably, optical experiments convincingly demonstrate the system's ability to produce accommodation-capable true 3D content, with a four-fold extension of FOV compared to a single SLM at an observation distance of 150 mm. Additional optical experiments highlight the successful integration of AR technology, an important component for automotive HUD.

1. Introduction

Augmented-reality (AR) displays provide users with realistic and immersive three- dimensional (3D) experiences, which opens up new opportunities for interacting with digital Content and the real world [1–4]. The most popular application of AR devices is the head- up display (HUD), which enhances driving safety and comfort by projecting critical driving information into the line of sight of a driver [5]. The field of view (FOV) in AR-HUD is a critical component because it directly affects the quality and quantity of visual information that a driver can perceive through the display. The magnifier-principle method is basically used to enlarge the image of a micro-display to generate a virtual image perceived by the driver at an observation distance [6]. Although this method can be considered successful in offering wide FOV, it suffers from a drawback in that a relatively long optical path is required between the optical components and display, which can increase the overall size and packaging volume of an HUD system. To realize a compact form factor with wide FOV, several alternative technologies have been explored, including the use of holographic optical elements (HOEs), liquid–crystal-based geometric phase lens, and pancake lens that folds the optical path. These elements still suffer from an unsatisfactory form factor. Additionally, large-area refractive optics-based approaches cause severe aberration and distortion of an image.

To overcome this limitation, some researchers have explored optical devices that do not require a long optical path and can provide wide FOV with a compact form factor. Recently, optical waveguide has been used as pupil expander, which has attracted increasing attention as an optical element for compact form factor and exit-pupil expansion. The waveguide extracts some of the light from the outcoupler and then directs it toward an observer. The remaining portion of light continues to propagate within the waveguide and interacts with the outcoupler again to extract an additional portion of light. This process is repeated multiple times, resulting in many replicas of the wavefield. Thus, expansion of the waveguide exit pupil allows reduction in the optical-path length and simultaneously extends FOV. The waveguides can be designed with different types of light-coupling methods and materials. Geometric waveguides use prisms and partially reflective mirrors to redirect and extract light from the waveguide [7,8]. Diffractive waveguides utilize

☆ This paper was recommended for publication by Prof Guangtao Zhai.

* Corresponding author.
E-mail address: jhahn@knu.ac.kr (J. Hahn).

https://doi.org/10.1016/j.displa.2023.102617
Received 19 October 2023; Received in revised form 1 December 2023; Accepted 13 December 2023
Available online 15 December 2023

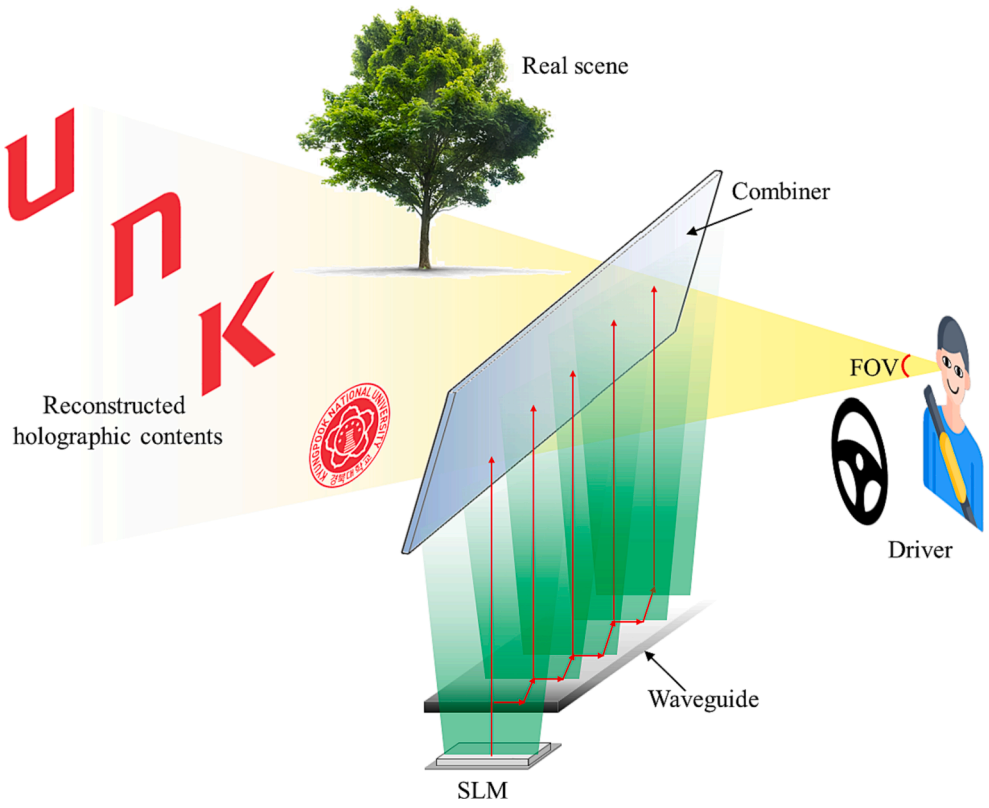

Fig. 1. System configuration of the proposed a lensless holographic waveguide HUD.

structures that diffract light, such as surface gratings, *meta*-surfaces, and HOEs, to achieve confinement and control of light propagation [9–11]. A curved waveguide provides the advantage in which achievable FOV is larger when the waveguide wraps around an observer [12]. However, although waveguides as exit-pupil expander provide a distinct advantage, they are limited in their ability to provide realistic and comfortable visual effects. Specifically, waveguide displays typically only provide two-dimensional (2D) images with infinite depth that is not affected by the optical-path variations introduced by the waveguide. Projection of an image with finite depth onto the waveguide causes some significant ghosting artifacts and noise because of the pupil-replication process. For augmented reality head-up displays (AR-HUD), which aim to provide information to drivers by integrating virtual content into real scenes, the limitation of generating only 2D virtual content with infinite depth causes a mismatch between real scenes and virtual content. This mismatch leads to various issues, such as visual fatigue, perceptual distortion, and a decrease in realism and immersion.

This mismatch can be alleviated by generating 3D virtual content that match the depth of the real scene. In this regard, several approaches have already been investigated such as multi depth display, autostereoscopic 3D display. Multi-depth techniques use a simple architecture, but the number of virtual image planes is limited and natural overlap is not sufficient. In addition, autostereoscopic approaches can generate virtual 3D content at an arbitrary depth using binocular disparity and integrate it with real scenes. However, the misalignment between the eye's convergence towards the virtual image and the accommodation of the eye lens in autostereoscopic displays causes the vergence-accommodation conflict (VAC) problem, resulting in visual discomfort [13]. Meanwhile, holography is generally considered as the most promising technology for solving the VAC problem completely because it provides essential 3D visual cues such as accommodation–vergence matching [14–17]. However, current holographic display experiences several challenges caused by the limited capability of spatial light modulator (SLM), which is an essential device for modulating the amplitude and phase of optical fields. Most SLMs commonly have limited space-bandwidth product (SBP), which leads to a trade-off between FOV and the eye-box size. Increasing SBP of SLM is a useful method for improving the quality of the reconstructed holographic image. Several approaches have been proposed to improve FOV and the eye-box size in a practical and cost-effective manner. One of these approaches is to spatially tile multiple SLMs. Although this method achieves higher SBP of the entire system, precise alignment and calibration of individual SLMs are required to generate seamless images without visible artifacts [18,19]. Another approach is to time- multiplex single SLM to improve SBP. This approach involves splitting a single hologram into multiple subholograms and sequentially displaying them in SLM [20,21]. However, this method requires a moving optical component to physically redirect the beam. Although the aforementioned methods can provide improved performance compared with single SLM, they also suffer from limitations in terms of spatio-temporal resolution as well as increased system complexity and cost.

In this paper, we introduce a lensless holographic waveguide display consisting of a waveguide with pupil replication, a phase only SLM, and a laser light source to generate true 3D holographic contents with extended FOV. The proposed system not only has a compact form factor by employing a waveguide as an optical component to extend the FOV, but also solve the mismatch problem between virtual content and real scene by generating accommodation-capable true 3D image over a full depth range. Our approach is fundamentally different from those of previous works in that the waveguide displays for pupil replication can extend the FOV of the observed image and provide true 3D images with full depth range. We proposed a formalized algorithm to calculate a computer generated hologram (CGH) based on a bold assumption and two constraints which is fundamentally different from conventional method, and validated the accommodation effect and FOV extension of the generated contents through numerical observation simulation and optical experiment. In particular, optical experimental results successfully reveal accommodation-capable true 3D content at an observation

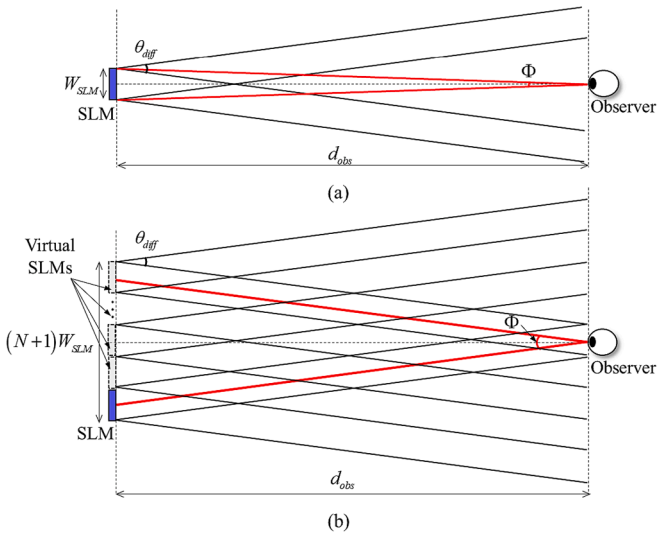

Fig. 2. Geometric relationship between FOV and width of SLM in a lensless holographic display for (a) single SLM case and (b) replicated virtual SLMs by the waveguide case.

distance of 150 mm in the waveguide-based system. Our system implements the FOV that is four times larger than that produced by a single SLM within an eye-box of 4.6 mm and offers contents at arbitrary depths over the full depth range. The experimental results are consistent with the supportive numerical observation simulation results. Additional optical experimental results provide evidence that AR technology, a key component in automotive HUD, operates effectively within the proposed system.

2. Optical design of the waveguide

Compared with the conventional waveguide display that uses a waveguide to expand the exit pupil, the major difference of our proposed lensless holographic waveguide display is that it provides accommodation-capable virtual 3D images. This difference is expected to significantly improve the perception experience of users by generating the accommodation-capable 3D content in real-world environments. Typically, a waveguide that is used as a pupil expander generates many shifted copies of wavefields with different optical paths inside the waveguide. These copies interfere with one another, resulting in a complex field in the final output because of the scrambled phase and intensity. This phenomenon is considered as an artifact that must be avoided to generate an accommodation-capable virtual 3D image. However, in our lensless holographic waveguide display system, we define each of the multiple shifted copies of the modulated wavefield generated inside the waveguide as replicated virtual SLMs. In this section, we present our geometric analysis that quantifies the improvement in FOV and eye-box attributable to the defined virtual SLMs. We also present the design of the optical configuration of the waveguide responsible for generating virtual SLMs.

Fig. 1 shows the system configuration of the proposed lensless holographic waveguide HUD. The architecture consists of a laser light source, single SLM, a waveguide used as a pupil expander, and a combiner. The plane wave from the laser source is modulated by SLM and projected onto the waveguide. Inside the waveguide, a portion of the modulated light is extracted, and the remaining light continues to propagate. This process is repeated several times within the waveguide to replicate virtual SLMs. The light extracted from the waveguide is merged with the light of an actual scene by the combiner and transferred to the observer. The combiner is a transflective mirror that does not have any optical power. In conventional waveguide displays, the exit pupil is expanded by the waveguide, but the mismatch problem between virtual content and real scene arise because they only produce images with infinite depth. On the other hand, the proposed holographic waveguide display combines holographic display and waveguide technology to generate an accommodation-capable 3D image with the extended FOV.

Providing large FOV of virtual images in the AR-HUD system is necessary for delivering immersive and engaging visual experiences. Traditionally, extending FOV has been accomplished by utilizing a magnifier such as a projection lens. Another approach employs multiple SLMs arranged in a tiled configuration, which requires complex optics and calibration among individual SLMs to generate seamless images without noticeable artifacts. These systems inevitably result in a bulky and complex system to extend FOV. Hence, in a lensless architecture, utilizing a waveguide for replicating multiple virtual SLMs is desirable from a form-factor standpoint to extend FOV. In our lensless architecture, virtual SLMs are replicated by the waveguide. An algorithm is employed to generate CGH with extended FOV under the assumption that predefined virtual SLMs function as a single ultra-high resolution SLM with same pixel density but with a very large number of pixels. A detailed description of the algorithm is provided in Section 3.

Fig. 2 shows the geometric relationship between FOV and the SLM width in a lensless holographic display. We consider the one-dimensional (1D) case because virtual SLMs are generated by the pupil expander in the horizontal direction. Single SLM with width W_{SLM} is expressed as $W_{SLM} = p \times M$, where p is the pixel pitch and M is the number of pixels in SLM. SLM modulates the phase of the incident plane wave under the constraints imposed by the diffraction-angle characteristics of SLM. The diffraction angle θ_{diff} is defined by

$$\theta_{diff} = 2\sin^{-1}\frac{\lambda}{2p}, \tag{1}$$

where λ is the wavelength. At observation distance d_{obs}, the observer can obtain reconstructed images with FOV. FOV Φ in the lensless holographic waveguide display is calculated as

$$\Phi = 2\tan^{-1}\frac{(N+1)W_{SLM}}{2d_{obs}}, \tag{2}$$

where N denotes the number of replicated virtual SLMs by the waveguide. Fig. 2(a) shows the case where $N = 0$, indicating that no virtual SLM exists due to the absence of a waveguide. A real single SLM provides a small FOV at the observation distance. Fig. 2(b) shows that N virtual SLMs with the same pixel pitch replicated by the waveguide provide an extended FOV at the observation distance. A conventional waveguide used as a pupil expander generates many shifted copies of wavefields with different optical paths inside the waveguide. These copies interfere with one another, resulting in a complex field in the final output because of the scrambled phase and intensity. This repetitive and complex wavefield does not result in FOV expansion but instead result in numerous ghost artifacts. In contrast to display systems that generate 2D images, in the holographic display systems, the wavefield diffracted from each pixel of SLM interferes with the projected virtual objects into arbitrary spaces. In other words, FOV is limited by the diffraction angle; thus, Eq. (2) is valid when FOV is less than or equal to the maximum diffraction angle of SLM. The number of replicated virtual SLMs required to achieve the maximum FOV in a lensless holographic waveguide display N_{diff} is calculated as

$$N_{diff} = \left\lceil\frac{\lambda d_{obs}}{pW_{SLM}}\right\rceil - 1, \tag{3}$$

where $\lceil\cdot\rceil$ denote the ceiling function or is known as the least integer function of real number. As the number of SLM replica increases, the intensity of the extracted wavefield reduces. Since the number of virtual SLMs replicated to achieve maximum FOV has limitation, a practical number of virtual SLMs needs to be adopted.

In a lensless holographic waveguide display, eye box is defined as the

area where the eye can observe the image with maximum FOV extended by the aforementioned virtual SLMs, as shown in Fig. 3. In fact, the input light wave modulated by SLM generates virtual SLMs through a replication process by the waveguide and provides reconstructed image of maximum FOV to the observer at an observation distance. As the eye position moves within the eye box, the SLM area required to reconstruct an image that provides maximum FOV changes. To implement the extended FOV, the angular range of the wave field generated by individual virtual SLM replicas reaching the observer within the eye-box is constrained to not overlap with the angular range of adjacent replicas. In other words, the proposed method performs FOV expansion by multiplexing the full angular information of the wavefield generated by the real SLM and numerous virtual SLM replicas. The limited angular range of the wave field is $\theta_{diff}/(N_{diff}+1)$ and is valid when $N \geq N_{diff}$. Multiplexing different angular information from adjacent neighboring replicas extends FOV within the eye-box. The multiplexed angular ranges of the SLM replicas converging on observer are marked in Fig. 3 with distinct colors, and the shared overlapping area is delineated as the eye-box. Angular multiplexing imposes limitations on the available angle range, consequently restricting the eye-box size as well. The limited eye-box size at the observation distance W_{eye} is calculated as

$$W_{eye} = \frac{2d_{obs}}{N_{diff}+1}\tan(\theta_{diff}/2). \tag{4}$$

The parameters for the horizontal direction actually used are $W_{SLM} = 4.59mm, d_{obs} = 150mm, p = 4.25\mu m$, and $\lambda = 520nm$. For $N = 0$, i.e. the simplest setup where a SLM is directly observed by an eye without any optics except the 4-f filter, FOV is calculated to be 1.75 degrees and the eye-box size is calculated to be 18.3 mm. In the proposed method, FOV is extended to 7.0 degrees by the virtual SLM replicas, but the eye-box size is reduced to 4.6 mm. In holographic displays, a trade-off exists between FOV and eye-box because SBP is constrained by the finite number of physical pixels of the SLM. Thus, when the generation of a virtual SLM replicas by a waveguide, FOV can be improved by a factor of four, but the eye-box size is reduced proportionally. Our method can be a valuable strategy to choose the reasonable balance between FOV and eye-box without the help of an optical lens such as a magnifier. In an AR-HUD that delivers an immersive experience, a wider FOV improves presence and realism, potentially justifying the sacrifice in eye-box size. Although eye-box size is limited, it is easy to expand the eye-box by applying eye-tracking technology. In this paper, only three SLM replicas are required to extend to the maximum FOV. To expand the eye-box, we generate four virtual SLM replicas where one is the room for eye-tracking. Because the area of effective SLM moves depending on the eye position, CGH needs to be updated to reflect the eye position detected by the eye-tracking technology.

Considering that conventional waveguide-based displays used as pupil expander only provide 2D images, the exit pupil of the projected image from SLM is expanded via a random replication procedure in the waveguide. To generate accommodation-capable holographic images in a waveguide-based display, we need to design the waveguide so that virtual SLMs created by the cloning procedure are defined. The waveguide structure is configured to define four virtual SLMs, as shown in Fig. 4, and the parameters of waveguide are designed to precisely position these virtual SLMs so that they do not overlap optically. The absence of overlap among virtual SLMs signifies that these virtual SLMs precisely modulate both the amplitude and phase of the wavefield necessary for generating a holographic image in an arbitrary space.

The waveguide described in this paper operates by placing partially tuned reflector and mirror in parallel to coherently extract the intensity of the replicated wavefield. The positions of virtual SLMs are determined by the spacing between the partial reflector and mirror as well as the angle between SLM and the waveguide. The plane wave from the laser source is modulated by SLM, and the waveguide extracts a portion of the modulated light and redirects the rest inside the waveguide. In this process, the waveguide must be designed so that the replicated wavefields do not overlap with one another. The replication pitch of the wavefield inside the waveguide RP is expressed as

$$RP = 2t \times \tan\theta, \tag{5}$$

where t is the thickness of the waveguide and θ_w is the angle between SLM and the waveguide. Therefore, to consider virtual and real SLMs as single SLM with ultra-high resolution, the replication pitch of the waveguide must be set to match the width of real SLM, which is denoted as W_{SLM}. The designed waveguide successfully creates virtual SLMs as intended but introduces optical-path-length error in the optical-axis direction. The optical-path-length difference among virtual SLMs l is calculated as

$$l = 2t/\cos\theta_w. \tag{6}$$

Accumulation of this optical-path difference occurs as the location where virtual SLM is generated moves farther away from real SLM. This phenomenon presents a challenge because it leads to artifacts in the proposed system. Therefore, our waveguide design is aimed at minimizing this optical-path difference, and we provide further compensation for it using our algorithm.

3. Algorithm for lensless holographic waveguide system

Conventional waveguide-based approaches with pupil replication provide a compact form factor in the system and sufficient eye-box size but suffer from the limitation of only providing 2D virtual images. We consider a novel method for generating CGH by modeling a lensless holographic waveguide system to create accommodation-capable 3D images with a full depth range while extending FOV. Fig. 5 shows the schematic diagram of the proposed lensless holographic waveguide system with extended FOV consisting of a waveguide, phase-only SLM, and a laser light source to generate true 3D holographic images with extended FOV.

The main idea of the proposed lensless holographic waveguide sys-

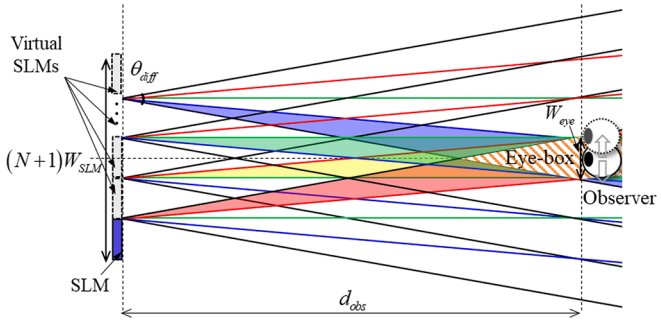

Fig. 3. Definition of an eye-box in a lensless holographic waveguide display that provides maximum FOV.

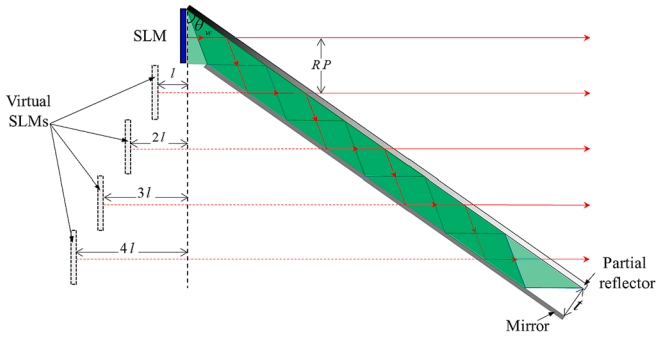

Fig. 4. The Structure of the waveguide that generates virtual SLMs.

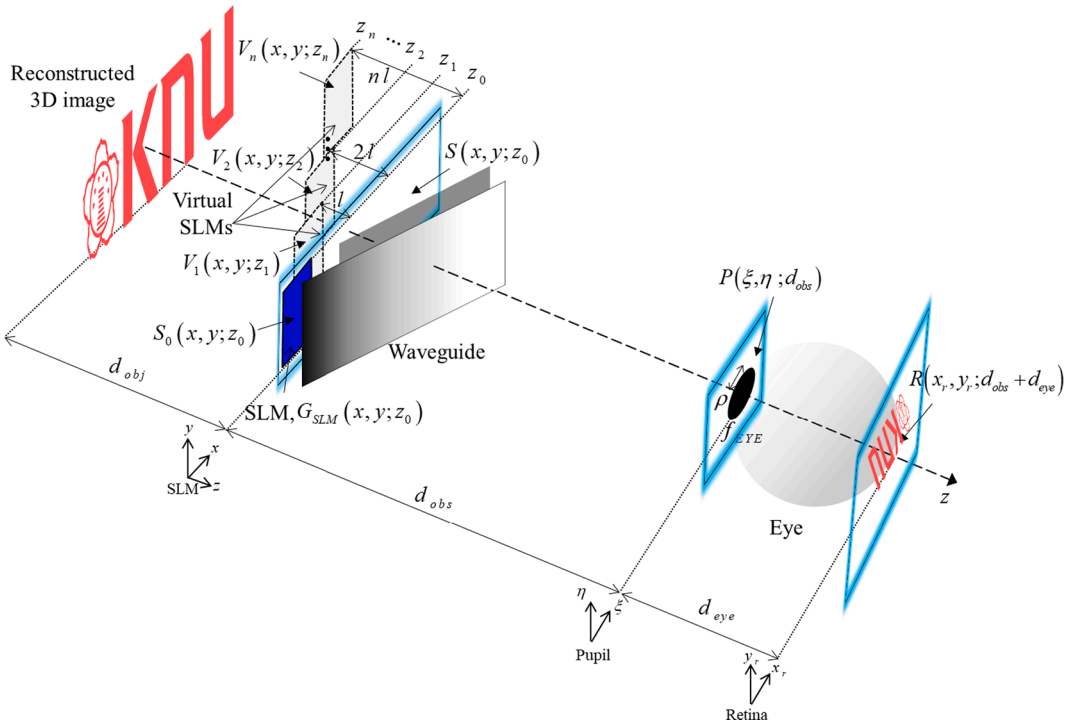

Fig. 5. Forward and inverse cascaded Fresnel transforms model for lensless holographic waveguide system with extended the FOV.

tem with extended FOV is to model the wavefield duplicated by the waveguide to be equal to generate virtual replicated SLMs. We assume that virtual replicated SLMs can be approximated using single ultra-high resolution SLM with some constraints. The single ultra-high resolution SLM has N times more pixels than the real SLM with the same pixel density. One of the constraints is that calculated CGH is loaded into physically real SLM, and the other constraint is that an optical path is added as much as l each time virtual SLM is replicated. This assumption represents the first step in our algorithm to extend FOV of a reconstructed image with a full depth range, breaking the limitation where traditional waveguide displays only expand the eye box.

On the basis of this assumption, we develop the forward and inverse cascaded Fresnel transform (CdFr and iCdFr, respectively) models, as shown in Fig. 5. The waveguide is replaced by several virtual replica SLMs; thus, the wavefield modulated by SLM is propagated in front of the eye only using the propagation formula in free space. The SLM plane $(x, y; z_0)$, pupil plane $(\xi, \eta\ ; d_{obs})$, and retina plane $(x_r, y_r; d_{obs} + d_{eye})$ are defined as shown in Fig. 5. We assume that the SLM plane is placed at the $z = z_0 = 0$ plane in the global coordinates. In our model, the observer focuses on the reconstructed holographic image, and the focal length of the eye lens f_{eye} is given by

$$f_{eye} = \frac{d_{eye}\left(d_{obs} + d_{obj}\right)}{d_{eye} + \left(d_{obs} + d_{obj}\right)}, \tag{7}$$

where d_{eye} is the distance between the eye lens plane and retina plane, d_{obs} is the observation distance between the SLM and pupil plane, and d_{obj} denotes the distance from SLM to the reconstructed image. The sign of d_{obj} is positive if the reconstructed image is located beyond the SLM, in a direction away from the observer, and negative if it is located between SLM and the observer. We mark the depth of the holographic image in Fig. 5 as a constant for convenience. However, in the algorithm, the depth of the holographic image is considered a variable to compute the hologram that simultaneously generates holographic images with various depths.

The mathematical formula between the wavefield $S(x, y; z_0)$ at the SLM plane and wavefield $R(x_r, y_r; d_{obs} + d_{eye})$ on the retina plane is described by CdFr and ICdFr [22,23]. We follow the definitions of CdFr and ICdFr models developed in our previous research from Refs. [22] and [23]:

$$\begin{aligned} &R\left(x_r, y_r; d_{obs} + d_{eye}\right) \\ &= CdFr\left\{S(x, y; z_0); d_{obs}, d_{eye}, f_{eye}, \rho\right\}, \end{aligned} \tag{8}$$

$$\begin{aligned} &S(x, y; z_0) \\ &= ICdFr\left\{R\left(x_r, y_r; d_{obs} + d_{eye}\right); d_{obs}, d_{eye}, f_{eye}\right\}, \end{aligned} \tag{9}$$

where ρ is the radius of the eye pupil. In a single SLM system without a waveguide, ICdFr generates CGH that reconstructs a holographic image in an arbitrary space. The observer successfully observes the reconstructed holographic image through CdFr. However, in our lensless holographic waveguide system, we need to develop an advanced algorithm that considers the characteristics of replicated virtual SLMs generated by the waveguide.

The nth replicated virtual SLM by the waveguide is formed by moving the optical axis in the opposite direction using accumulated optical-path-length difference nl. Because of this constraint, the wavefield $S(x, y; z_0)$ in the SLM plane calculated by Eq. (9) should be transferred to the plane of virtual replicated SLMs. We can obtain the wavefield on the virtual SLM using the angular spectrum method (ASM) [24]. The ASM equation is defined as

$$ASM\{u(x, y; z), d\} = \mathscr{F}^{-1}\left\{\mathscr{F}\{u(x, y; z)\}\exp\left(j2\pi d\sqrt{1/\lambda^2 - 1/f_x^2 - 1/f_y^2}\right)\right\} \tag{10}$$

where $F\{\cdot\}$ and $F^{-1}\{\cdot\}$ denote the Fourier transform and inverse Fourier transform, respectively, $u(x, y; z)$ is the wavefield on an arbitrary plane parallel to the $(x, y; z_0)$ plane, f_x and f_y are spatial frequencies. To obtain the complex wavefield on the n th virtual SLM, wavefield $S(x, y; z_0)$ in the SLM plane propagates by nl.

The complex wavefield at nth virtual SLM replicated in the horizontal direction $V_n(x, y; z_n)$ is calculated as

$$V_n(x,y;z_n) = ASM\left\{S(x,y;z_0)rect\left[\frac{x+(N/2-n)W_{SLM}}{W_{SLM}}\right],z_n\right\}, \quad (11)$$

where $rect\{\cdot\}$ denotes the rectangular function. By this function, the wavefield at the SLM plane is cropped to the same number of sampling points as the real SLM. The wavefield obtained in the area where real SLM is located occurs in the case of $n = 0$ in Eq. (11), and the wavefield $S_0(x_0,y_0;z_0)$ is calculated as

$$S_0(x,y;z_0) = S(x,y;z_0)rect\left[\frac{x+(N/2)W_{SLM}}{W_{SLM}}\right]. \quad (12)$$

Another constraint in our bold assumption is that SLMs defined by the waveguide are virtual SLMs as replicas of real SLM. Because N virtual SLMs are replicas of the real SLM, the wavefiled calculated by Eq. (11) is not modulated by the nth virtual SLM. To overcome this constrain, a solution is derived that superposes the wavefield $S_0(x,y;z_0)$ and N wavefields $V_1(x,y;z_1) \sim V_N(x,y;z_N)$, allowing them to be modulated by the real SLM. In our algorithm, the computation of CGH that is ultimately encoded on the real SLM $G_{SLM}(x,y;z_0)$ is performed as follows:

$$G_{SLM}(x,y;z_0) = S_0(x,y;z_0) + \sum_{n=1}^{N} V_n(x+nW_{SLM},y;z_n). \quad (13)$$

The number of horizontal sampling points of the complex wavefield $S(x,y;z_0)$ is $(N+1)\times M$. The number of sampling points of the complex wavefields $S_0(x,y;z_0)$, $V_n(x,y;z_n)$, and $G_{SLM}(x,y;z_0)$ is cropped by the rectangular function and is equal to M, which is the number of pixels of the real SLM.

Conventional waveguide-based approach that uses pupil replication has been proven to be adaptable to HUD applications, providing a compact form factor as well as sufficient eye-box size but only 2D virtual images with an infinite depth. The projection of an image with finite depth onto the waveguide causes some significant ghosting artifacts and noise due to the pupil-replication process. The human eye uses various depth cues such as vergence and accommodation distance to perceive the depth of an object. Virtual objects with fixed depth generated by the system cause mismatch with the real scene. The depth mismatch between virtual content and real scene can disrupt the integration of them, confusing the human visual system. The depth mismatch problem between real scene and virtual content can be eliminated by providing the accommodation-capable virtual image reconstructed over the entire depth range. To realize a 3D virtual image with accommodation capability, we consider a novel method to extend FOV instead of expanding the eye box through pupil replication in a waveguide display.

Fig. 6(a) shows numerical observation results obtained from a conventional waveguide- based holographic display used as a pupil expander. The first column of Fig. 6(a) presents the configuration of a conventional waveguide used as an exit pupil expander, which simply generates a myriad of shifted copies of the image projected from the SLM. The second column shows an image with a finite depth of 20 cm, and the third column shows an image with infinite depth. In the conventional method, the image with an infinite depth is normally observed without artifacts, but artifacts such as superimposed ghost noise occur in the image with a finite depth of 20 cm when displayed through a waveguide. Generating only an image with a fixed depth does not provide accommodation effect and causes the mismatch problem between virtual content and real scene. On the other hand, the first column of Fig. 6(b) presents the configuration of the accommodation-capable waveguide, which generates virtual SLMs without overlapping each other. CGH used in our holographic waveguide display is calculated by replacing the pupil replication function with a function that extends FOV of the entire image. This algorithm makes possible the generation of an image at a target depth by considering the waveguide. The second and third columns in Fig. 6(b) show images with a finite depth of 20 cm and with an infinite depth, respectively, observed using the proposed method. We can clearly verify that the proposed method successfully

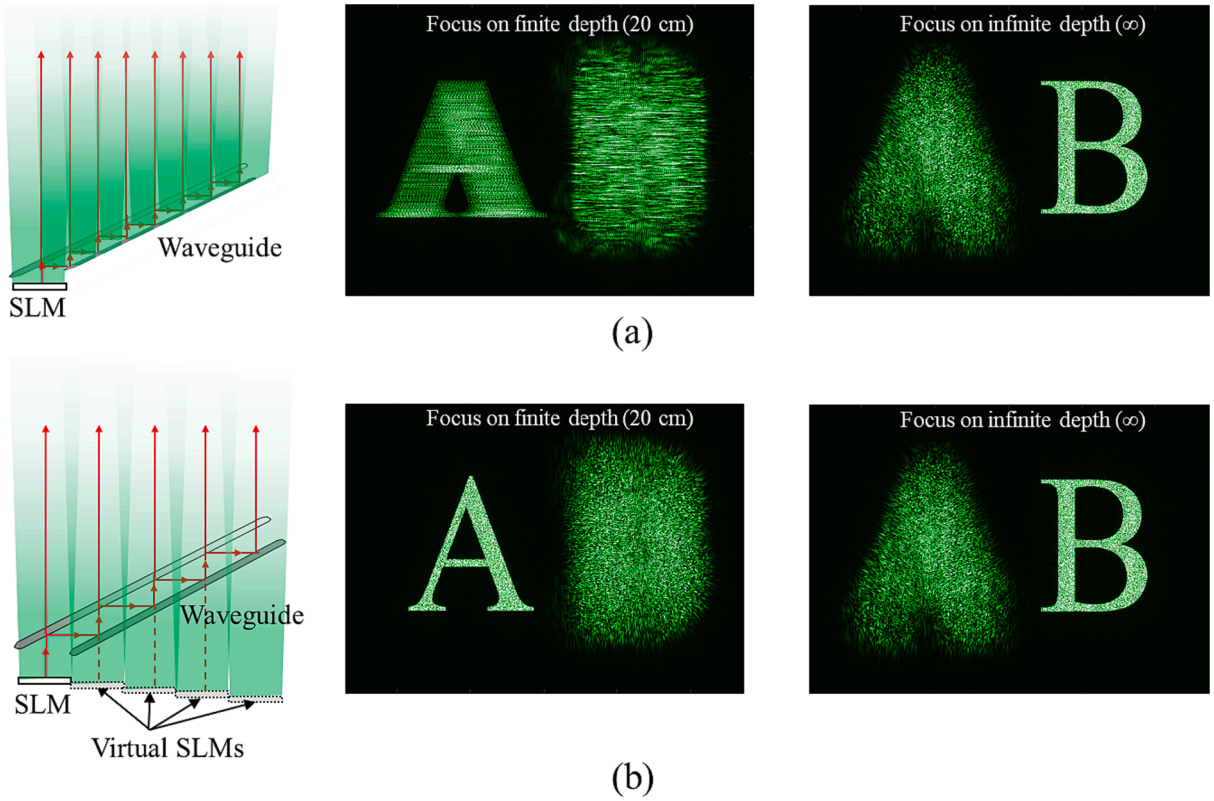

Fig. 6. Numerical observation results of a holographic waveguide display using (a) conventional waveguide and (b) accommodation-capable waveguide.

reconstructs the infinite- and finite-depth holographic images through the waveguide. The proposed waveguide-based holographic display with a full depth range provides an accommodation effect and solves the mismatch problem between virtual content and real scene that occurs in the conventional display.

CGH generated by applying the proposed algorithm for the lensless holographic waveguide system successfully realizes accommodation-capable images in the numerical observation simulations. In the simulation, CGH is calculated by applying depth-map CGH, a well-known hologram-generation algorithm that simultaneously generates images at multiple depths [25]. The numerical observation results have verified that the depth range of the reconstructed images spans from zero to infinity from the perspective of the observer, and FOV is extended through the replication of virtual SLMs by the waveguide. Fig. 7 shows the numerical simulation results in the accommodation-capable holographic display with a pupil expander. The target image is a signature of the Kyungpook National University where the symbol is an image located 120 mm away from the observer, and letters "K, "N,", and "U" are 250 mm, 650 mm, 10,000 mm away from the observer, respectively as shown in Fig. 7(a). Fig. 7(b)–(e) show the numerical simulation results for observations at a distance of 150 mm from the SLM plane. The observation results are displayed on the retina plane. The entire target image has FOV of approximately 7.0 degrees horizontally. When the eye focuses on the target depth of a particular letter, the rest of the letters at different depths become blurred, providing an accommodation effect to the observer. The detailed parameters used in the simulation are listed in Table 1.

Table 1
System parameters.

Parameter	Symbol	Value
Wavelength of light source	λ	520 nm
Width of SLM	W_{SLM}	4.59 mm (H) 8.16 mm (V)
Pixel pitch of SLM	p	4.25 μm
Observation distance	d_{obs}	150 mm
The number of replicated virtual SLMs	N	4
Thickness of waveguide	t	3 mm
Angle between SLM and waveguide	θ_w	37.4°
The optical-path-length difference among virtual SLMs	l	7.55 mm
Distance between pupil plane and retina plane	d_{eye}	25 mm
Radius of pupil	ρ	2 mm

4. Experimental results

An optical experiment is set up to verify the lensless holographic waveguide system where the proposed method is applied on an optical table, as shown in Fig. 8. The optical experiment consists of a laser light source, a spatial filter, single SLM, and a waveguide. The spatial filter is used improve the spatial coherence of the light source, and the apertures are used is to control the size of the collimated beam. A reflection-type phase-only SLM (model name: HX-7322) with a pixel pitch of 4.25μm, 1080 × 1920 resolution is used, and a 520 nm green laser is used as the light source. The f-number of the camera is 1.8, the focal length of the prime lens is 7 mm, and the aperture size is the calculated to be 3.9 mm. The aperture size of camera is a value that corresponds to the average pupil size of human eye. Currently, the limited fill factor of the commercial liquid crystal on the silicon panel used as SLM creates an unmodulated signal that inevitably introduces DC noise at the center of the entire FOV. This noise is a major obstacle in observing holographic images and should be removed. However, it is difficult to completely eliminate unmodulated DC noise caused by the limited fill factor of practical SLM. In the experiment, we optically remove the high-order and DC noise using a 4f system.

The optical experiments have shown that images can be generated at arbitrary depths from zero to infinity from the observer, which confirms that CGH generated by the proposed algorithm can display 3D images with a full depth range that are capable of accommodation on waveguide-based display. Fig. 9 shows the experimental results of the accommodation- capable waveguide display. To verify the proposed method, we show the reconstructed images at various depths while providing extended FOV using virtual replicated SLMs. The camera is adjusted to focus on the designated target depth of each image, as shown in Fig. 7(a). The accommodation effect of the captured images can be observed through the focusing and blurring that corresponds to the focal length of the camera. When the camera is focused on the symbol, the symbol appears sharp while letters "K," "N," and "U" become blurred

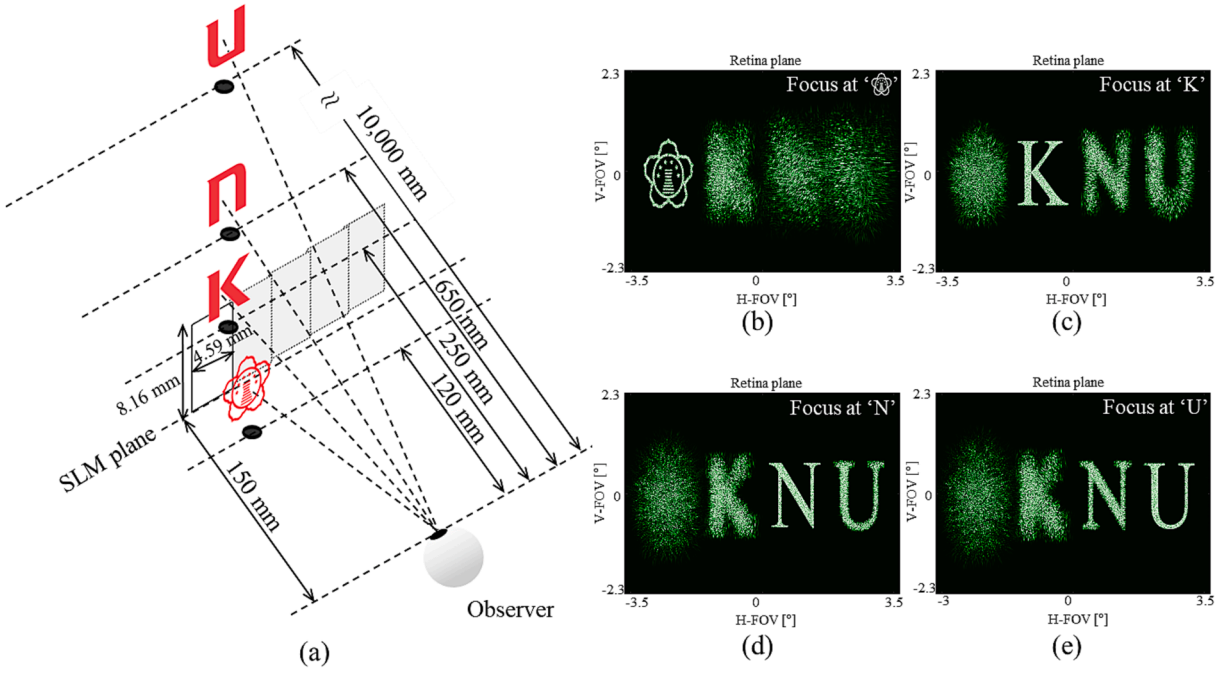

Fig. 7. Numerical observation results. (a) Original depths of the target objects with full depth range and numerical observation results when the eye is focused at (b) "symbol," and letters (c) "K," (d) "N," and (e) "U".

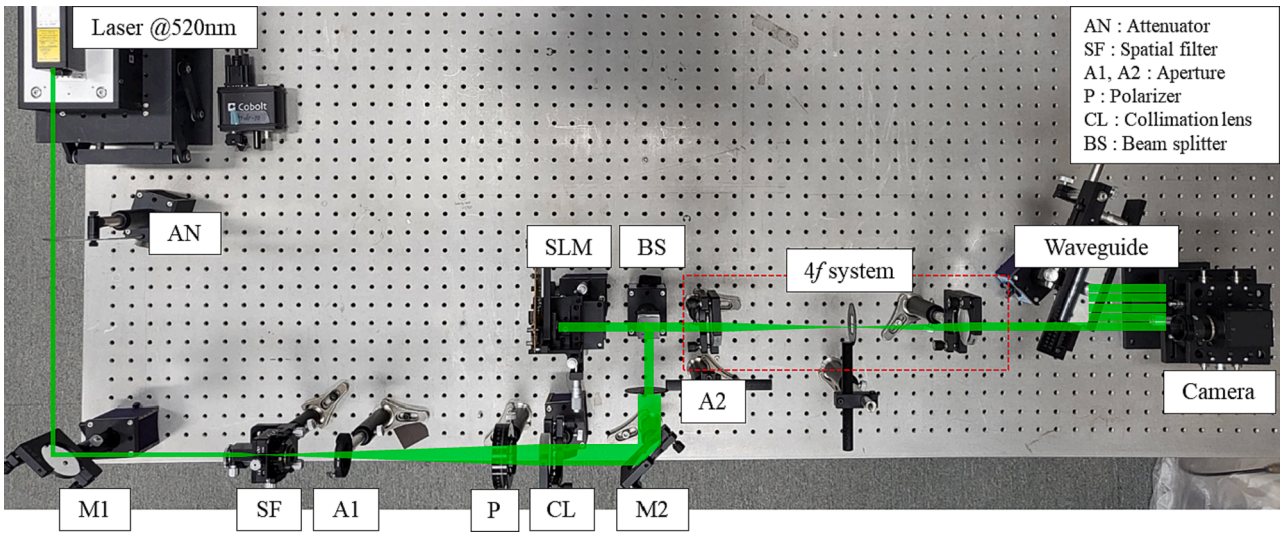

Fig. 8. Experimental set-up.

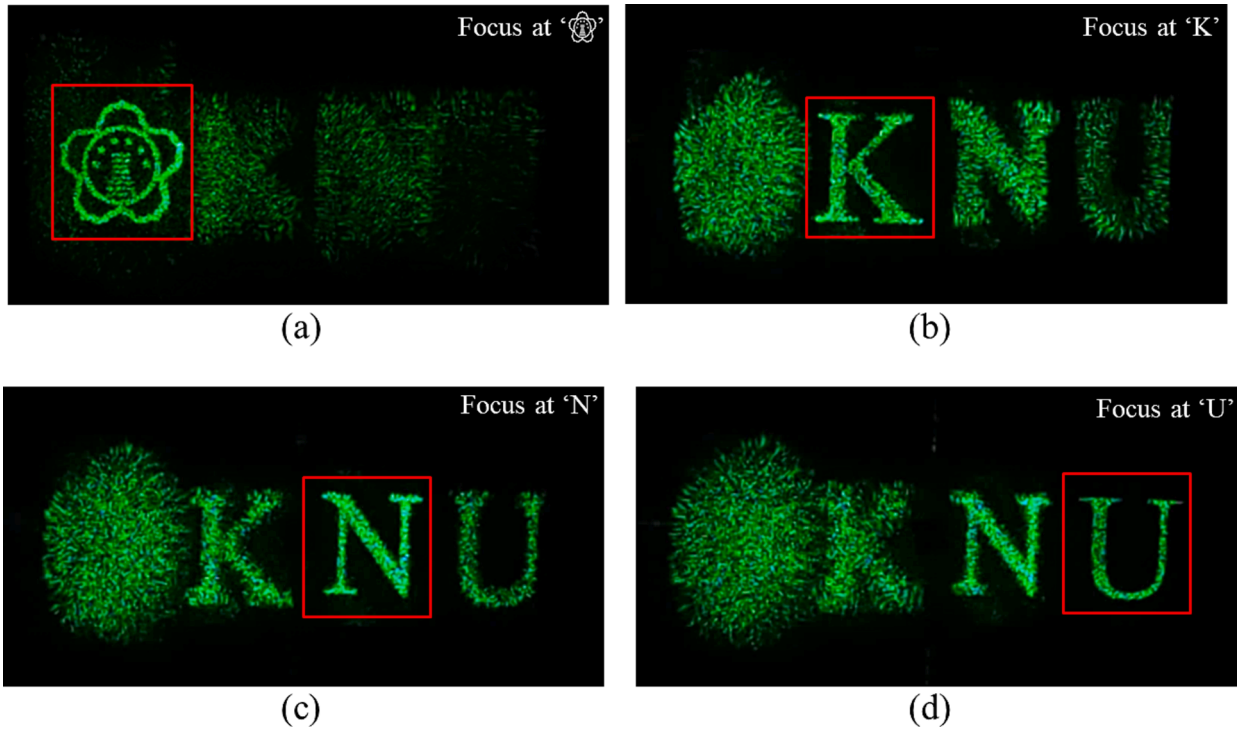

Fig. 9. Experimental results of the accommodation-capable waveguide display.

[Fig. 9(a)]. Conversely, when the camera is focused on letter "K," letter "K" becomes sharp while the symbol and letters "N" and "U" appear blurred [Fig. 9(b)]. Similarly, the same conditions are observed when the camera is focused on letters "N" and "U" [Fig. 9(c) and (d), respectively]. These results are consistent with the numerical simulation results and provide an accommodation effect to the observer. These results are consistent with the outcomes of the numerical simulations, confirming our successful experimental validation to provide accommodation-capable images to the observer. We must note that the waveguide- based display delivers high-quality images without a ghost image not only when the image is displayed at infinite depth but also at finite depth.

AR technology indeed overlays digital information or content onto the real world to enhance the perception of user and interaction with the environment. AR technology plays a pivotal role in automotive HUD owing to its potential to significantly improve safety, enhance driving experience, and offer critical information to drivers without causing distractions. The experimental results applying AR technology shown in Fig. 10 inspire that our system solves the mismatch between virtual content and real scenes. In the experiment, virtual content was created identical to the results in Fig. 9, and four types of real objects were prepared at the same depth positions as the virtual images generated at different depths. The four real objects were a die placed at a distance of 120 mm from the observer, a tiger cattle keyring placed at a distance of 250 mm, a cup placed at a distance of 650 mm, and one of the authors located at a distance of 10,000 mm. In Fig. 10, the results are captured by changing the camera's focus from near to far. The in-focus part of the virtual content is indicated by a red box, and the in-focus object among

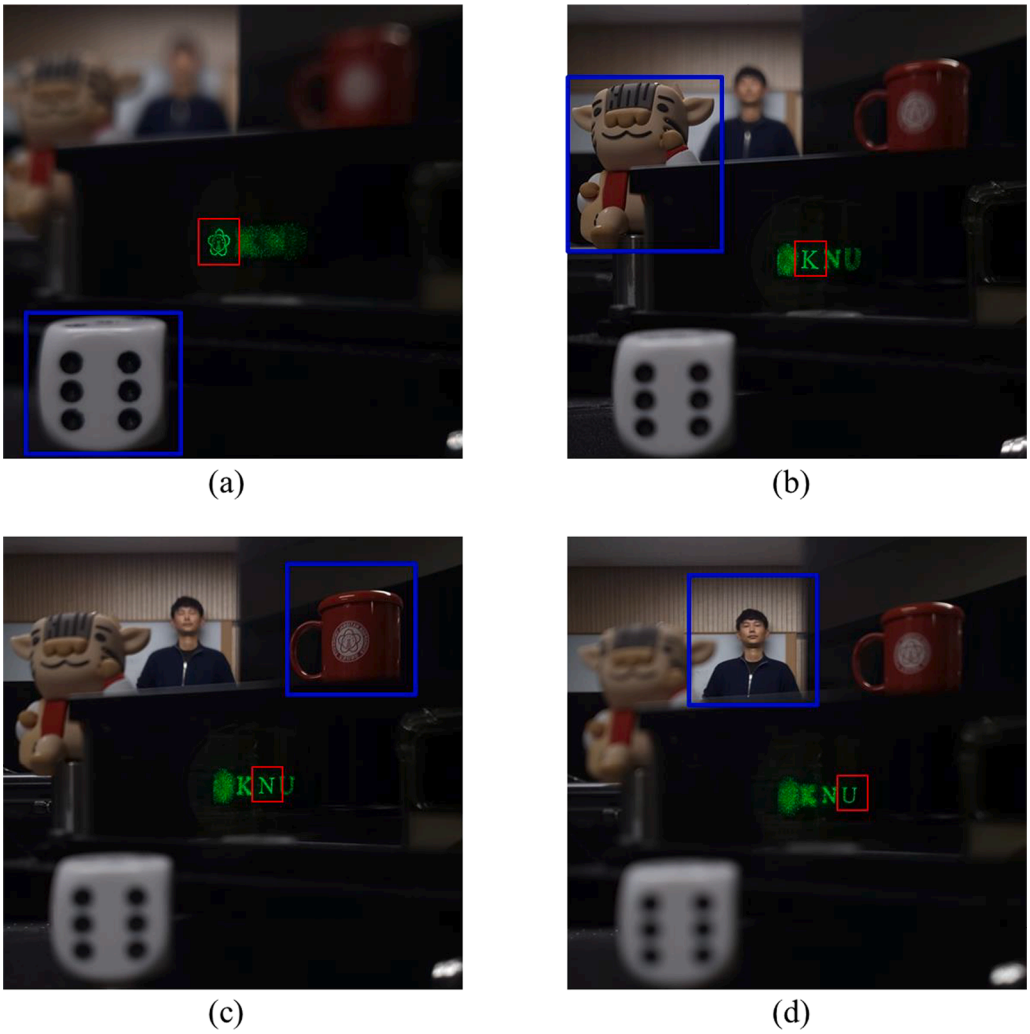

Fig. 10. AR application results (see Visualization) when the camera focuses (a) a dice, (b) a tiger cattle keyring, (c) a cup and (d) human (one of the authers).

the real objects is indicated by a blue box. When the camera is focused at a distance of 120 mm from the observer, the dice among the real objects and the logo among the virtual content are sharp, while all others are blurred [Fig. 10(a)]. When the camera focuses on the tiger cattle keyring among the real objects, only the letter "K" becomes clear and the rest becomes out of focus [Fig. 10(b)]. Similar results are observed when the camera focuses on a real object, such as the cup or one of the authors [Fig. 10(c) and (d)].

Fig. 11 shows another experimental results on an entire toy train image with the same depth reconstructed using real and replicated virtual SLMs. The reconstructed holographic image consists of the engine of the toy train and three tender cars marked with letters "A," "B," and "C." The real and virtual SLMs replicated by the waveguide indicate the engine and three tender cars of the entire toy train, respectively. The captured image shows the engine and three tender cars seamlessly connected into a single toy train with no discernible joints or artifacts. The displayed horizontal FOV of the entire toy train is about 7.0 degrees. Because horizontal FOV of the holographic image reconstructed by single SLM at the same observation distance is 1.75 degrees, FOV in the proposed lensless holographic waveguide display is extended by approximately four times.

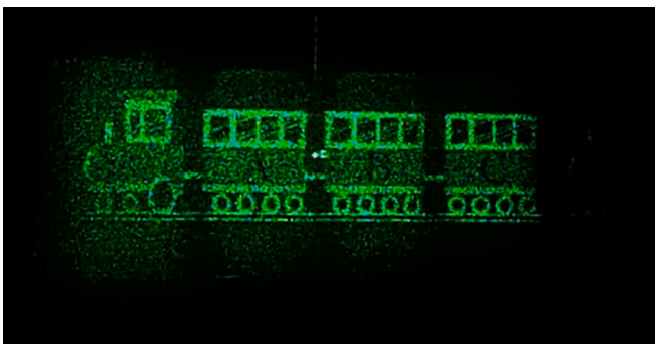

Fig. 11. Experimental result of the entire image with the same depth reconstructed by real SLM and replicated virtual SLMs.

5. Discussion

The proposed system utilizes a lensless direct view configuration, avoiding aberrations induced by optical lenses like magnifiers, and boasts a compact form factor. However, it is important to acknowledge that the system has limitations as its FOV is constrained by the pixel pitch of the SLM. FOV is a particularly important performance in AR-HUD because the AR-HUD need to be able to display enough information to see not only the lane you are driving in, but also the lanes to your left and right.To fully display all three lanes, FOV in AR-HUD is required to be at least 15 degrees horizontally and 5 degrees vertically. Although the proposed system successfully achieved a maximum horizontal FOV

of 7.0 degrees on an optic table, there is still significant potential for improvement FOV. In our system, the vertical FOV is not expanded, so the vertical FOV does not change and the vertical FOV is 3.1 degrees. Since it has been verified that horizontal FOV can be extend, it is clear that vertical FOV can also be extended with the proposed method. To achieve this, it is necessary to apply 2D waveguide to replicate SLM in both directions. The 2D waveguide consists of two waveguides, one that replicates the SLM in the horizontal direction and the other that sequentially replicates the horizontally duplicated SLM in the vertical direction. This paper emphasizes a focus on the future innovation of micro-display technology, highlighting the novelty of the lensless architecture. Efforts are ongoing in academia and industry to develop and manufacture sub-micrometer pixel pitch panels, which could be a solution to improve FOV in the long run, raising expectations for AR-HUD. If an SLM with a pixel pitch of 2 μm is used, FOV of 15 degrees will be realized for the green laser light source at the observation distance. As the pixel pitch decreases, the number of virtual SLMs replicated by the waveguide will increase, which is calculated as Eq. (2). If the SLMs have the same resolution, the width of the SLMs will also be smaller, so the thickness of the designed waveguide and the angle with the SLMs will be smaller, resulting in a much more compact form factor. Also, in this paper, the eye-box size is set to 4.6 mm, but the eye-box size can be further optimized by Eq. (4) as the parameters of the SLM are changed. In this regard, the proposed system not only provides accommodation-capable virtual images with an extended FOV but also has potential to cooperate with future technological advancements in SLM technology to ultimately realize an AR-HUD.

6. Conclusion

In this paper, we propose a lensless holographic waveguide display consisting of a laser light source, a single SLM, a waveguide to generate true 3D holographic images with an extended FOV. We defined each of the multiple shifted copies of the modulated wavefield generated inside the waveguide as a replicated virtual SLM and optically designed a waveguide in which the replicated virtual SLMs were defined. We proposed a formalized algorithm based on a bold assumption and two constraints which is fundamentally different from traditional waveguide displays, and validated the accommodation effect and FOV extension of the generated contents through numerical observation simulation and optical experiment. In particular, optical experimental results successfully reveal accommodation-capable true 3D content at an observation distance of 150 mm in the waveguide-based system. Our system implements FOV that is four times larger than that produced by a single SLM within an eye-box of 4.6 mm and offers contents at arbitrary depths over the full depth range. The experimental results are consistent with the supportive numerical observation simulation results. Additional optical experimental results provide evidence that AR technology, a key component in automotive HUD, operates effectively within the proposed system. Eventually, the maximum horizontal FOV of 7.0 degrees is realized using the phase only SLM with 4.25 μm pixel pitch. It is a natural fact that FOV increases as the pixel size decreases, so it will be possible to implement a HUD with a commercially reasonable FOV by reducing the pixel size. In the near future, we will explore ways to apply eye tracking technology to track eye position and update CGH to increase the limited eye-box.

Funding

This research was supported by Alchemist Project grant funded by Korea Evaluation Institute of Industrial Technology (KEIT) & the Korea Government (MOTIE) (Project Number: 1415179744, 20019169).

Disclosures

The authors declare that they have no known competing financial interests or personal relationships that could have appeared to influence the work reported in this paper.

CRediT authorship contribution statement

Woonchan Moon: Conceptualization, Validation, Writing – original draft. **Hosung Jeon:** Formal analysis, Visualization. **Sehwan Na:** Software. **Hwi Kim:** Project administration. **Joonku Hahn:** Supervision, Funding acquisition.

Declaration of Competing Interest

The authors declare that they have no known competing financial interests or personal relationships that could have appeared to influence the work reported in this paper.

Data availability

Data will be made available on request.

Appendix A. Supplementary material

Supplementary data to this article can be found online at https://doi.org/10.1016/j.displa.2023.102617.

References

[1] J. Xiong, E.L. Hsiang, Z. He, T. Zhan, S.T. Wu, Augmented reality and virtual reality displays: emerging technologies and future perspectives, Light Sci. Appl. 10 (2021) 1–30.
[2] K. Yin, E.L. Hsiang, J. Zou, Y. Li, Z. Yang, Q. Yang, P.C. Lai, C.L. Lin, S.T. Wu, Advanced liquid crystal devices for augmented reality and virtual reality displays: principles and applications, Light Sci. Appl. 11 (2022).
[3] N. Xu, F. Yu, J. Xu, D. Jin, H. Feng, Z. Xu, Q. Li, Y. Chen, HUDNet: A dynamic calibration method for automotive augmented reality head-up-displays, Displays 78 (2023), 102453.
[4] R. Li, Y.V. Chen, L. Zhang, Z. Shen, Z.C. Qian, Effects of perception of head-up display on the driving safety of experienced and inexperienced drivers, Displays 64 (2020), 101962.
[5] C.M. Bigler, M.S. Mann, P.A. Blanche, Holographic waveguide HUD with in-line pupil expansion and 2D FOV expansion, Appl. Opt. 58 (2019) 326–331.
[6] O. Cakmakci, J. Rolland, Head-worn displays: a review, J. Display Technol. 2 (2006) 199–216.
[7] D. Cheng, Y. Wang, C. Xu, W. Song, G. Jin, Design of an ultra-thin near-eye display with geometrical waveguide and freeform optics, Opt. Exp. 22 (2014) 20705.
[8] M. Xu, H. Hua, Methods of optimizing and evaluating geometrical lightguides with microstructure mirrors for augmented reality displays, Opt. Exp. 27 (2019) 5523.
[9] C.P. Chen, L. Mi, W. Zhang, J. Ye, G. Li, Waveguide-based near-eye display with dual-channel exit pupil expander, Displays 67 (2021), 101998.
[10] B.C. Kress, I. Chatterjee, Waveguide combiners for mixed reality headsets: a nanophotonics design perspective, Front. Opt. Photon. 10 (2021) 41–74.
[11] J. Xiao, J. Liu, Z. Lv, X. Shi, J. Han, On-axis near-eye display system based on directional scattering holographic waveguide and curved goggle, Opt. Exp. 27 (2019) 1683.
[12] C.T. Draper, P.A. Blanche, Holographic curved waveguide combiner for HUD/AR with 1-D pupil expansion, Opt. Exp. 30 (2022) 2503.
[13] D.M. Hoffman, A.R. Girshick, K. Akeley, M.S. Banks, Vergence-accommodation conflicts hinder visual performance and cause visual fatigue, J. Vis. 8 (2008) 1–30.
[14] S. Tay, P.A. Blanche, R. Voorakaranam, A.V. Tunç, W. Lin, S. Rokutanda, T. Gu, D. Flores, P. Wang, G. Li, P.S. Hilaire, J. Thomas, R.A. Norwood, M. Yamamoto, N. Peyghambarian, An updatable holographic three-dimensional display, Nature 451 (2008) 694–698.
[15] J. Hong, Y. Kim, H-J. Choi, J. Hahn, J-H. Park, H. Kim, S-W. Min, N. Chen, B. Lee, Three- dimensional display technologies of recent interest: principles, status and issues [invited], Appl. Opt. 50 (2011) 87–115.
[16] M.Y. He, D. Wang, Y. Xing, Y.W. Zheng, H.L. Zhang, X.L. Ma, R.Y. Yuan, Q. H. Wang, Compact and lightweight optical see-through holographic near-eye display based on holographic lens, Displays 70 (2021), 102104.
[17] H. Yanagihara, T. Kakue, Y. Yamamoto, T. Shimobaba, T. Ito, Real-time three-dimensional video reconstruction of real scenes with deep depth using electro-holographic display system, Opt. Exp. 27 (2019) 15662.
[18] W. Moon, H. Jeon, S. Park, S. Kim, H. Kim, J. Hahn, Seamless holographic image generation for a multi-vision system, J. Inf. Disp. 23 (2022) 287–298.
[19] H. Sasaki, K. Yamamoto, K. Wakunami, Y. Ichihashi, R. Oi, T. Senoh, Large size three-dimensional video by electronic holography using multiple spatial light modulators, Sci. Rep. 4 (2014) 4–11.
[20] Y. Takaki, M. Nakaoka, Scalable screen-size enlargement by multi-channel viewing-zone scanning holog- raphy, Opt. Exp. 24 (2016) 18772.

[21] J. Li, Q. Smithwick, D. Chu, Full bandwidth dynamic coarse integral holographic displays with large field of view using a large resonant scanner and a galvanometer scanner, Opt. Exp. 26 (2018) 17459.
[22] J. Roh, K. Kim, E. Moon, S. Kim, B. Yang, J. Hahn, H. Kim, Full-color holographic projection display system featuring an achromatic Fourier filter, Opt. Exp. 25 (2017) 14774.
[23] D. Im, E. Moon, Y. Park, D. Lee, J. Hahn, H. Kim, Phase-regularized polygon computer-generated holograms, Opt. Lett 39 (2014) 3642.
[24] J.W. Goodman, Introduction to Fourier Optics, third ed., Roberts and Company Publishers, 2005.
[25] S. Park, J. Lee, S. Lim, M. Kim, S. Ahn, S. Hwang, S. Jeon, J. Jeong, J. Hahn, H. Kim, Wide-viewing full-color depthmap computer-generated holograms, Opt. Exp. 29 (2021) 26793–26807.